Received: 6 September 2022 | Revised: 22 December 2022 | Accepted: 26 December 2022

DOI: 10.1002/jmor.21574

RESEARCH ARTICLE

JOURNAL OF morphology WILEY

Formation of a fringe: A look inside baleen morphology using a multimodal visual approach

Megan L. Vandenberg[1,2] | Karly E. Cohen[1,2] | Robert D. Rubin[3] | Jeremy A. Goldbogen[4] | Adam P. Summers[1,2] | E. W. Misty Paig-Tran[5] | Shirel R. Kahane-Rapport[5]

[1]Department of Biology, University of Washington, Seattle, Washington, USA

[2]Friday Harbor Laboratories, University of Washington, Friday Harbor, Washington, USA

[3]Santa Rosa College, Santa Rosa, California, USA

[4]Hopkins Marine Station, Stanford University, Pacific Grove, California, USA

[5]California State University, Fullerton, California, USA

Correspondence
Shirel R. Kahane-Rapport, California State University, Fullerton, CA, USA.
Email: Skahane-rapport@fullerton.edu

Funding information
National Science Foundation Postdoctoral Research Fellowship in Biology; American Cetacean Society; National Science Foundation Division of Integrative Organismal Systems; Stephen and Ruth Wainwright Endowment Fellowship

Abstract

Filter-feeding has been present for hundreds of millions of years, independently evolving in aquatic vertebrates' numerous times. Mysticete whales are a group of gigantic, marine filter-feeders that are defined by their fringed baleen and are divided into two groups: balaenids and rorquals. Recent studies have shown that balaenids likely feed using a self-cleaning, cross-flow filtration mechanism where food particles are collected and then swept to the esophagus for swallowing. However, it is unclear how filtering is achieved in the rorquals (Balaenopteridae). Lunging rorqual whales engulf enormous masses of both prey and water; the prey is then separated from the water through baleen plates lining the length of their upper jaw and positioned perpendicular to flow. Rorqual baleen is composed of both major (larger) and minor (smaller) keratin plates containing embedded fringe that extends into the whale's mouth, forming a filtering fringe. We used a multimodal approach, including microcomputed tomography (μCT) and scanning electron microscopy (SEM), to visualize and describe the variability in baleen anatomy across five species of rorqual whales, spanning two orders of magnitude in body length. For most morphological measurements, larger whales exhibited hypoallometry relative to body length. μCT and SEM revealed that the major and minor plates break away from the mineralized fringes at variable distances from the gums. We proposed a model for estimating the effective pore size to determine whether flow scales with body length or prey size across species. We found that pore size is likely not a proxy for prey size but instead, may reflect changes in resistance through the filter that affect fluid flow.

KEYWORDS
baleen, filter morphology, micro-CT, SEM

Megan L. Vandenberg and Karly E. Cohen are co-first authors.

1 | INTRODUCTION

Filtration is an ancient feeding mechanism that independently evolved many times across many clades (Stiefel, 2021). Filter-feeders span seven orders of magnitude in body length and include choanoflagellates, ascidians, flamingos, many fishes, and baleen whales. The gigantic modern filter-feeders can be divided into three groups based on the morphology of their filters: stratified filters (oarfishes and megamouth sharks), flattened filters (manta/mobula rays and whale sharks), and bristle filters (baleen whales and basking sharks). Oarfish and megamouth sharks have stratified, comb-like filters, with distinct hardened surface structures (Paig-Tran & Summers, 2014; Roberts, 2012). The flattened filter group (manta and devil rays and whale sharks) have filters that resemble a series of repeating wing-like structures attached to a central support raphe (Paig-Tran et al., 2013). Bristle filters are composed of keratinous, often calcified, elongated structures (resembling the bristles on a household broom) that are embedded into epithelial tissues (Matthews & Parker, 1950; Pivorunas, 1977). These filters are suspended from the jaws (baleen whales) or gill arches (basking sharks) and are oriented perpendicular to the incoming flow.

Mysticete whales are the most recent radiation of gigantic marine filter-feeders and their fringe-type filter, commonly known as baleen, is a defining characteristic. The "fringe" is found on the distal edge of the baleen plate with respect to the gum line and is created by a row of keratinous fringes. Extant mysticetes are divided into two clades with distinct filter morphologies: the ram feeding balaenids, composed of four species, and the lunging balaenopterids or rorquals, with nine species. Notably, there has been some debate regarding the inclusion of gray whales (*Eschrichtius robustus*) within the rorqual grouping. Although gray whales had not been considered part of the true rorquals for some time (Gatesy et al., 2013; Sasaki et al., 2005), the most recent phylogenetic analyses firmly place gray whales within the family Balaenopteridae (Árnason et al., 2018; Lammers et al., 2019; McGowen et al., 2020). Baleen plate length, spacing, and number varies between the two par-orders and likely corresponds to variations in prey size, prey capture behaviors, and filtration mechanisms (J. A. Goldbogen et al., 2017; Werth, 2000).

The morphology of a filter dictates the mechanism by which particles are collected and retained. For example, a filter oriented perpendicular to flow usually functions as a dead-end sieve (Rubenstein & Koehl, 1977). Much like a colander captures pasta, particles larger than the pore size of a filter become trapped, while particles smaller than the filter pore exit through the filter with the water. There are inherent challenges with dead-end sieving systems: the filter rapidly clogs and can only retain particles greater than the filter pore size (Rubenstein & Koehl, 1977). Direct sieving is a mechanism often attributed to baleen whales, particularly in rorquals. Indeed, the earliest known filtering whale, *Coronodon havensteini*, likely developed teeth that worked as a simple sieve, known as interdental filter-feeding slots which formed as the diastema grew between molar-like teeth (Geisler et al., 2017). More recent work suggests that early rorquals may have transitioned from having only teeth to a combination of baleen and teeth to just baleen (Ekdale & Deméré, 2022; Gatesy et al., 2022).

A second mechanism of particle collection, cross-flow filtration, is a method in which the particles that do not transit through the filter are retained and moved across the filter surface. The principal water flow, with entrained particles, moves over the filter at an oblique angle to the incoming flow. The flow takes a sharp turn to exit through the filter, establishing a tangential shearing flow that pushes captured particles downstream (Bhave, 1997). In other words, flow that does not pass through the filter immediately creates a self-clearing mechanism that moves particles from the filter to a point of collection. This cross-flow filtration may work with a dead-end sieve, or there may be pores larger than the particle size that are partially occluded by vortices induced by the tangential flow (vortical cross-step filtration). In either case, the tangential shearing moves particles toward a collection point (Cohen et al., 2018; Storm et al., 2020). Cross-flow filtration was suggested by J. Goldbogen et al. (2007) as a possible mechanism of filtration in rorquals, due to the similarity of estimated flow speed and Reynolds number to that of suspension feeding fishes employing cross-flow filtration (J. Goldbogen et al., 2007; Sanderson et al., 2001). However, in these mechanisms, some particles never encounter the filter, allowing particles even smaller than the pore size to be retained (Sanderson et al., 2001; Sanderson et al., 2016). The fluid dynamics underlying these mechanisms are still not well understood.

The historical and widely accepted mechanism for food collection in the mysticete whales has long been sieve filtration; where zooplankton (krill, copepods, etc.) larger than the pore size created by the baleen are caught and then secondarily scraped off the filter using the enormous tongue. Some have suggested other mechanisms such as backwashing, head shaking, or using the muscularized ventral grooves to actively move engulfed water back and forth over the baleen (J. A. Goldbogen et al., 2017; Werth, 2001). The bowheads have well-defined muscular tongues, but the rorquals have poorly muscled, almost flaccid tongues that are likely incapable of such dynamic and finely-controlled motion (Lambertsen, 1983; Werth & Ito, 2017). The rorquals do have muscles in the ventral groove blubber that may contribute to the clearing of the ventral pouch (J. A. Goldbogen et al., 2017). An interesting possibility for drawing water out of the mouth in both radiations of whales is that water flow on the labial side of the baleen, moving faster than the water in the mouth, creates a venturi effect that assists the tongue or contracting ventral groove blubber in removing water (Werth, Rita, et al., 2018). It is unclear how sieve filtration and the subsequent clearing of the filter is achieved in the Balaenopteridae.

Furthermore, sieving was recently demonstrated to be an unlikely mechanism for ram feeding balaenids, shown both by computational models and testing fresh samples of baleen (Potvin & Werth, 2017; Werth & Potvin, 2016). Both right (*Eubalaena* spp.) and bowhead whales (*Balaena mysticetus*) feed using continuous and slow ram filtration and have extraordinarily long, dark gray to black baleen plates that can be more than 4 m in length (Werth, 2000; Werth, Rita, et al., 2018). Water moving through the oral cavity is

funneled into specialized channels, either along the tongue (anteroposterior tongue [APT] channel) or lip (anteroposterior lip [APL] channel), effectively passing over the baleen rack in a perpendicular fashion (Werth & Potvin, 2016). This suggests prey capture is via cross-flow filtration, as the models showed particles both directly contacting the filter surface (cross-flow) and bypassing the filter completely (vortical cross-step filtration).

While great leaps have been made to link the filter morphology and filtration mechanisms in the balaenid whales, there are still holes in our understanding of the filter morphology and filtration mechanism in rorquals. Rorqual whales have substantial variation in foraging mechanics, baleen morphology, and the scaling of their control surfaces and engulfment capacity (Cade et al., 2016; Jensen et al., 2017; Kahane-Rapport & Goldbogen, 2018). Rorquals lunge filter-feed in a two-step process (Shadwick et al., 2019). Initially, they engulf a massive volume of prey-laden water while executing a high-energy lunge. This water is then filtered through the racks of baleen, ensuring prey is retained in the mouth. Rorquals repeat these lunges hundreds of times per day, targeting dense swarms of prey (Goldbogen et al., 2015). Gray whales utilize both lunge filter feeding and benthic floor suction feeding behaviors to capture prey (Brower et al., 2017).

Although isometric theory predicts that the engulfment capacity should scale in proportion to body length cubed (length^3) and that baleen area should scale in proportion to body length squared (length^2), baleen whales exhibit hyperallometry (positive allometry) of the engulfment capacity and hypoallometry (negative allometry) of their baleen area (Kahane-Rapport et al., 2020; Werth, Potvin, et al., 2018). Larger whales engulf disproportionately large volumes of water which are subsequently filtered out through a disproportionately smaller baleen area, resulting in increased filter time for larger whales (Kahane-Rapport et al., 2020). Rorquals have short baleen plates compared to the balaenids, with a fringe that forms a dense mat (Jensen et al., 2017). The effective size of the pores in the baleen must influence both the size of the prey collected and the speed at which water moves through the system. However, defining the pore size is not a straightforward task. The filter fringes pile on top of one another, creating a dynamic, 3-dimensional structure through which water moves. Though there is no single pore size, this structure, a layer of fibers overlapping one another, is commonly found in industrial filters. The tools for calculating pore size in industry could be useful as a proxy for estimating pore size in baleen.

Our goals for this study are to use both wetted and dry baleen samples in a (1) multimodal approach to visualize and describe the hierarchical anatomy of baleen across five species of rorquals that span an order of magnitude in body length and two orders of magnitude in mass; (2) use contrast CT scanning and scanning electron microscopy to reveal internal baleen anatomy, the surface of the fringes and plates, and the interface where fringes exit plates; (3) quantify the gross and microscopic changes in filter anatomy to make comparisons to body length across species; and (4) use a proposed model of effective pore size to determine whether flow through the baleen and the back pressure scale with body length or prey size.

In this paper, we follow the baleen terminology used in Williamson (1973) with minor exceptions (see Supporting Information: Table 1). Hereafter, in line with Williamson, we define the entire keratinous filtering structure that is attached to the upper jaw of mysticetes as a baleen rack, or simply baleen, and the keratinous plates as baleen plates, which are made up of major (bigger and on the labial side of the rack) and minor (smaller and on the lingual side of the rack) plates. We define the baleen rack as having fringes, which is the collective make up of all the filtering strands that emerge from the plates, with each individual strand defined as a fringe.

2 | MATERIALS AND METHODS

Wet Specimen Collection—The freshly frozen sections of baleen were opportunistically sampled by The Marine Mammal Center (TMMC) Necropsy team in Sausalito, California, USA. The section of juvenile blue whale (*Balaenoptera musculus*) baleen was collected in Daly City, San Mateo, CA on September 26, 2016 (C-517). Juvenile fin whale (*Balaenoptera physalus*) baleen was collected on April 24, 2021, Fort Funston, San Francisco, CA (C-669). The section of juvenile humpback whale (*Megaptera novaeangliae*) baleen was collected in Eureka, Humboldt, CA, on September 23, 2019 (C-634). The section of juvenile gray whale (*Eschrichtius robustus*) baleen was collected in Richmond, Contra Costa, CA on May 8, 2020 (C-646). For all wet specimens, we received only a section of the baleen rack, and it is unknown where along the rack it is from, which side of the mouth, or the total body length of the whale. We removed two minor plates from the blue, fin, and humpback whale specimens.

Dry Specimen Collection—The dry sections from the common minke whale (*Balaenoptera acutorostrata*) (R-1) and the gray whale (R-2) baleen came from the personal collection of Robert Rubin (co-author on manuscript; hereafter referred to as R. R.) and had been preserved dry for more than 30 years. These specimens will be deposited at the Burke Museum of Natural History and Culture, in Seattle, Washington, USA. Additionally, we measured adult specimens of blue (72562), fin (54761), humpback (54806), gray (85979), and minke whale (54808) baleen from the Natural History Museum of Los Angeles County (NHMLAC) in Vernon, California, USA. For the dry specimens from the NHMLAC, total body length of the whale is known (Table 1). For the dry specimens from the collection of R. R., the total body length of the whale is unknown. For all dry specimens, we sampled only a section of the baleen rack, and it is unknown where along the rack it is from or which side of the mouth.

Macro Photography—We rehydrated whole, fresh frozen baleen sections from each of the three wet specimens (C-517, C-669, C-646), and the two dry sections (R-1 and R-2) in a seawater table for 2–3 h. We photographed each rehydrated section of baleen in lateral, lingual, and labial views using a Canon EOS 5D DSLR outfitted with a 100 mm macro lens. We photographed other regions of interest, including the interface between the keratin plate of the baleen and the free fringe extending from the plate using a 180 mm macro lens.

TABLE 1 Specimen table of all samples used in this study.

Species	Specimen ID	Condition	Age	Collection	Body length (m)
Balaenoptera musculus	C-517	Wet	Juvenile	TMMC	NA
Balaenoptera musculus	72562	Dry	Adult	NHMLAC	22.6
Balaenoptera physalus	C-669	Wet	Juvenile	TMMC	NA
Balaenoptera physalus	54761	Dry	Adult	NHMLAC	19.8
Eschrichtius robustus	R-2	Dry	Adult	R.R./Burke	NA
Eschrichtius robustus	85979	Dry	Adult	NHMLAC	14.0
Eschrichtius robustus	C-646	Wet	Adult	TMMC	NA
Megaptera novaeangliae	54806	Dry	Adult	NHMLAC	10.6
Megaptera novaeangliae	C-634	Wet	Juvenile	TMMC	NA
Balaenoptera acutorostrata	R-1	Dry	Adult	R.R./Burke	NA
Balaenoptera acutorostrata	54808	Dry	Adult	NHMLAC	8.0

Note: Including species, specimen ID, condition of the sample, age of the whale and where the sample came from. TMMC is The Marine Mammal Center, NHMLAC is the Natural History Museum of Los Angeles County, R. R. refers to the personal collection of Robert Rubin, and Burke refers to the Burke Museum of Natural History and Culture.

Computed Tomography (μCT and CT)—We fixed the wet minor plates from the blue, fin, and humpback whales in a solution of 10% formalin for 24 h. The minke and gray major plates were not fixed since they were received as dried specimens. After fixation, we dehydrated all five species' minor plates through a gradual stepwise ethanol series up to a 70% EtOH solution over the course of 3 days, before staining with a 3% solution of phosphotungstic acid (PTA, Sigma Aldrich CAS 12501-23-4) in 70% EtOH for 2 weeks. Once stained with PTA, we packed each plate for CT in a sealed plastic bag packed into a PLA 3D-printed tube, wrapped with cling film, and attached to a brass base. We scanned the minor plates of all species with the Bruker 1173 Bruker micro-CT machine at the Karel F. Liem Bio Imaging Center at Friday Harbor Laboratories, Friday Harbor, WA (Table 2). We reconstructed each scan in Nrecon (Bruker, 2005–2011) and segmented and measured the resulting data in 3D Slicer (version 4.11) using the Slicermorph extension module (Rolfe et al., 2021). All specimen scans are available for download at morphosource.org (Table 2). Additionally, the fresh frozen sections of baleen were scanned at the University of Washington Computed Tomography Facility, using a NSI X5000 CT machine (Table 3). The fresh frozen sections were not stained.

Scanning Electron Microscopy (SEM)—A single minor plate from the blue, fin, and humpback whales was prepared for SEM. One major plate from the pieces of minke and gray whales (dry sections from R. R.'s personal collection) was prepared for SEM. All five samples were removed from 70% ethanol, patted dry, and placed in −80°F for 3 hours. Once completely frozen, the plates were scored with a scalpel and the area of interest was snapped away from the rest of the plate. We imaged two sections from each species; one section of the keratinous plate was removed from the base (proximal end) and one section was taken from the edge of the plate at the interface between the keratin plate and free fringe (distal end of the plate). Samples were processed through a second gradual stepwise dehydration series from 70% to 100% ethanol, with 10 min in each stage. We placed each of the baleen plate samples in individual clean glass containers and covered them with a solution of hexamethyldisilazane (HMDS) for an hour, allowing the HMDS to diffuse through the cell boundaries under a fume hood before pipetting out 90% of the solution. The remaining solution evaporated while the specimen air dried completely. The baleen samples were then placed on a carbon paper-coated metal stub before sputter coating with gold palladium in the Cressington SPI Sputter 12121 (SPI Supplies/Structure Pro) for 60 s. We imaged each specimen using the SEM (Jeol Neoscope JCM-5000) at 15 kv at the Karel L. Liem Bio Imaging Center at Friday Harbor Laboratories.

Quantification of Baleen Morphology—We haphazardly sampled locations along the baleen sections available to us; however, we aimed to sample the longest plates from the sections available. The data provided herein reflects representative samples for the entirety of the baleen rack but may not include the maximum and minimum of baleen present in each specimen (Table 1). Instead, we provide these measurements as a comparative basis for rorqual baleen.

Fringe diameters were measured either from CT scans using 3D Slicer or with a caliper, depending on the specimen and scan quality. The diameters of 25 minor plate fringe were measured using Slicer from the computed tomography scans of blue (C-517), fin (C-669), humpback (C-634), and gray (R-2 and C-646) whales, in addition to 25 major plate fringe diameters of the minke whale (R-1). In Slicer, this was done using the maximum threshold that encompassed the entirety of the plate and fringe. We selected an axial slice through the free fringe that was perpendicular to the majority of the fringe being measured. Only fringe 90 degrees to the slice were used for measurement purposes as fringe are oriented in different directions. Diameter of the fringe was measured using the ruler tool available in

TABLE 2 Samples collected by The Marine Mammal Center Necropsy Team or from Robert Rubin's personal collection, now at the Burke Museum of Natural History and Culture.

Species	Age	Specimen ID	Fixation method	Stain	Voxel Size (μm)	Exposure (ms)	Morpho-source ARK #
Balaenoptera musculus	Juvenile	C-517	10% formalin	3% PTA in 70% EtOH	25.5	950	ark:/87602/m4/489406
Balaenoptera physalus	Juvenile	C-669	10% formalin	3% PTA in 70% EtOH	13.4	1011	ark:/87602/m4/489487
Eschrichtius robustus	Unknown	R-2	Dried and rehydrated	3% PTA in 70% EtOH	25.5	1017	ark:/87602/m4/494303
Megaptera novaeangliae	Juvenile	C-634	10% formalin	3% PTA in 70% EtOH	8.5	940	ark:/87602/m4/489666
Balaenoptera acutorostrata	Unknown	R-1	Dried and rehydrated	3% PTA in 70% EtOH	25.5	908	ark:/87602/m4/494116

Note: Table contains age, ID number, fixation method, stain, three-dimensional pixel (voxel) size for the reconstructed image, and exposure in ms. All specimens were scanned with X-ray source voltage of 55 kV, X-ray source intensity of 133 μA, and scanning resolution of 2048. All specimens were scanned at the Karel F. Liem Bio Imaging Center at Friday Harbor Laboratories, Friday Harbor WA and are available on Morphosource (see the Data Availability Statement section).

Slicer markups; we drew a line from the exterior most pixel of the fringe to the opposite exterior most pixel in which that line also crossed the center of the fringe. If the fringe was not perfectly symmetrical, we chose the widest part of the fringe to measure.

We note that the following measurements were taken from dried baleen plates; this is not the natural environment of baleen plates which would hydrate, bend, and displace the fringe and plates during filtration.

We measured 25 haphazardly selected major plate fringe diameters for blue (72562), fin (54761), gray (85979), humpback (54806), and minke (54808) whales, and also the minor plate fringe diameters for a minke whale (54808), using calipers. We measured 1 mm beyond the point of fringe emergence from the keratin plate (Figure 1). We then found the average diameter and standard deviation of all of the fringes measured of both the major plate and minor plates (Table 4).

Plate thickness was measured using a caliper for the major and minor plates of blue (72562), fin (54761), gray (85979), humpback (54806), and minke (54808) whales. Thickness was measured from both the lingual and labial sides of each major plate from the center of the plate, as thickness changes along the depth of the major plate. For the minor plates, this was done by placing the caliper on either side of the base of the plate just past the gum and measuring the thickness of the middle of the plate (Figure 1). We haphazardly measured the thickness of 10 major plates and 10 minor plates from each specimen, and then calculated the average thickness and standard deviation (Table 4).

We measured the plate spacing for both the major and minor plate of dry specimens, 10 spaces in blue (72562), 10 in fin (54761), 23 in gray (85979), 10 in humpback (54806), and 13 in minke (54808) whales (Table 1) and calculated the average spacing and standard deviation (Table 4). We used a caliper to measure the distance from the center of the labial edge of the plate to the center of the labial edge of the next adjacent plate (Figure 1).

We measured the length of at least eight major and minor plates from dry specimens (Table 1). These were measured using a ruler, from the gum line of the specimen to the tip of the plate, before the emergence of the fringes, on each plate measured (Figure 1). The tip of the plate was determined as the furthest part of the plate from the gum excluding the fringes. We then took the average and standard deviation of the lengths of both the major and minor plates (Table 4).

We measured the number of fringes per cm of baleen from the dry specimens by taking a photograph of three baleen major plates and three baleen minor plates and then counting the number fringes in a 1 cm^2 area in ImageJ (Version 1.53t) (Schneider et al., 2012) (Table 1). We then found the average and standard deviation of the fringe densities for both the major and minor plates (Table 4).

Effective pore size—In the literature of filter design, hydraulic pore diameter directly affects both pressure drop and filter selectivity. We estimated hydraulic pore diameter (d_h) of baleen using the Kozeny-Carman equation for spherical filter media beds (Ripperger et al., 2013) (Equation 1). The equation for hydraulic diameter (d_h) (mm) is,

Species	Age	Specimen ID	kV	μA	Morpho-source ARK #
Balaenoptera musculus	Juvenile	C-517	145	270	ark:/87602/m4/490280
Balaenoptera physalus	Juvenile	C-669	148	340	ark:/87602/m4/494308
Megaptera novaeangliae	Juvenile	C-634	148	340	ark:/87602/m4/494308

Note: Table contains ID number, X-ray source voltage in kilovolts (kV), X-ray source intensity in micro-amperes (μA), scanning resolution, and exposure in ms. All specimens were scanned with 128.3 voxel size (three-dimensional pixel) in microns, scanning resolution of 2048, and an exposure (ms) of 100. No fixation method or stain was used. All specimens were scanned at the Computed Tomography facility at the University of Washington, Seattle, WA, USA, and are available on Morphosource (see Data Availability Statement).

TABLE 3 All juvenile specimens were collected by The Marine Mammal Center Necropsy Team.

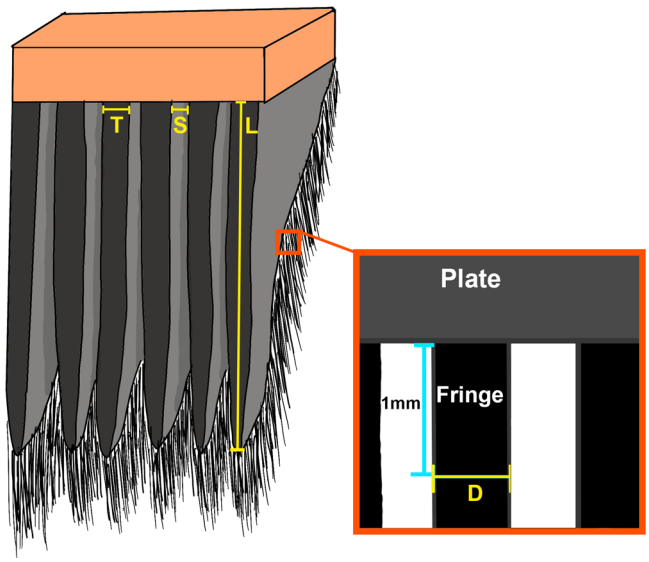

FIGURE 1 Section of baleen showing the location of measurements. T indicates plate thickness, S indicates plate spacing, D indicates fringe diameter taken at 1 mm away from the plate, L indicates plate length.

$$d_h = \frac{4\varepsilon}{(1-\varepsilon) * S_v}, \quad (1)$$

where (ε) is the void fraction of the fringe mat and Sauter diameter (S_v) is the inner interacting fringe surface. Void fraction (ε) is the volume of empty space between the fringes and where water can flow through. The Sauter diameter (S_v) is a ratio of the mean volume to the mean surface area of the filter media (ds, mm^3/mm^2) which accounts for the inner surface of the filter medium—that is, the portion of the baleen interacting with the fluid (Equation 2). We calculated the surface area and volume of the mat using the average measured fringe diameter for each species from Table 4.

$$S_v = \frac{6}{d_s}. \quad (2)$$

To effectively apply this equation, we made two assumptions: (1) although this equation applies to spherical beds and fringes are elongated structures, the fringes are circular when viewed in cross section and therefore can be used as a proxy when estimating the surface area of the filter media, and (2) this equation applies only to dead-end filtration, one of the currently predicted modes of filtration for rorquals, though it is entirely possible that whales are using another mechanism of filtration. This parameter can provide an effective estimator of relative pressure drop across the filter and relative pore size.

We have a sufficiently large volume of filter fringe to estimate this parameter for three species: blue, fin, and humpback whales. To calculate the hydraulic diameter (d_h) we segmented two segmentation nodes in 3D slicer. The first node contained a threshold encompassing only the fringes; the second node included the fringes plus all voxels in the same volume as the first node (i.e., negative space). We then calculated the volume of the whole cube and the volume and surface area of the fringes using segment statistics (d_s). Subtracting these two values left us with a total void fraction (ε).

Statistical methods—To test for significant differences across selected morphological parameters of baleen, we ran an ANOVA in R 4.1.2 (R Core Team, 2021) using the packages "tidyverse" (Wickham et al., 2019), "dplyr" (v1.0.8; [Wickham et al., 2022]), and "rstatix" (v0.7.0; [Kassambara, 2021]). When the ANOVA indicated significant differences among the group, we conducted a Tukey's HSD analysis to determine where the differences occurred. We used linear models to investigate the relationship between major fringe diameter, minor fringe diameter, major plate thickness (lingual and labial), minor plate thickness, major plate spacing, minor plate spacing, major plate length, and minor plate length, and body length, using museum specimens (Table 4). All variables were log10 transformed, which is standard practice for investigating ecological scaling relationships (Kerkhoff & Enquist, 2009). We analyzed a number of measurements per morphological feature, dependent on availability in the sample, for each species of whale ($n = 1$) to establish a baseline framework to compare whale size to baleen measurements.

3 | RESULTS

Rorqual baleen attaches along the length of the upper jaw (Figures 1–6). Baleen plates vary in size and are oriented transversely. Large, "major" plates are situated labially, with smaller, "minor" plates lingual to them. For all species, there are more minor plates than major plates and more fringes per cm in the minor plates compared to the major plates (Table 4). Inside each plate are thick-walled, hollow fringes extending from the gums through the plate (Figures 7–10).

TABLE 4 Species, specimen ID, total length (m) of the specimen measured, major and minor average number of fringes per cm and s.d, average plate spacing (mm, s.d), major and minor average plate thickness (mm, s.d), major and minor plate average fringe diameter (mm, s.d), major and minor average plate length (mm, s.d.) for each section of baleen used in this study. All whales in this table were adult specimens from the NHMLAC.

Species	Specimen ID	Average minor plate length (mm)	Average major plate length (mm)	Average minor plate fringe diameter (mm)	Average major plate fringe diameter (mm)	Average minor plate thickness (mm)	Average major plate thickness labial (mm)	Average major plate thickness lingual (mm)	Average minor plate spacing (mm)	Average major plate spacing (mm)	Average minor plate no. of fringes per cm	Average major plate no. of fringes per cm	Total body length (m)
Balaenoptera musculus	72562	169.7 ± 7.1	634.5 ± 27.8	0.4 ± 0.1	1.0 ± 0.2	2.0 ± 0.2	4.9 ± 1.0	3.8 ± 0.8	9.5 ±1.6	12.9 ± 2.7	18.0 ± 1.6	13.3 ± 1.6	22.6
Balaenoptera physalus	54761	70.7 ± 13.3	583.1 ± 38.7	0.6 ± 0.3	0.8 ± 0.2	2.3 ±1.1	3.6 ± 0.8	3.6 ± 0.6	5.8 ± 1.0	8.7 ± 1.3	17.8 ± 3.5	9.5 ± 2.2	19.8
Escrichtius robustus	85979	29.8 ± 8.5	287.9 ± 55.8	0.5 ± 0.1	0.8 ± 0.1	1.5 ± 0.1	5.3 ± 0.3	4.7 ± 0.4	5.1 ± 1.0	8.4 ± 1.1	12.0 ± 2.0	8.2 ± 1.5	14.0
Megaptera novaeangliae	54806	55.5 ± 22.2	568.6 ± 47.8	0.3 ± 0.1	0.5 ± 0.1	1.3 ± 0.3	2.8 ± 0.6	3.0 ± 0.5	3.4 ± 0.3	8.4 ± 1.5	28.3 ± 2.0	16.5 ± 2.2	10.6
Balaenoptera acutorostrata	54808	25.5 ± 7.3	196.9 ± 15.8	0.2 ± 0.1	0.7 ± 0.1	0.8 ± 0.2	1.4 ± 0.3	1.5 ± 0.2	2.0 ± 0.4	3.3 ± 0.4	27.0 ± 2.6	22.6 ± 3.3	8.0

The plate breaks away from these fringes along an edge some distance from the gum, leaving the fringes to form the dense mat (Figures 7 and 8). Contrast computed tomography (CT) scanning revealed the cylindrical fringes are not uniformly mineralized and are encased in a sheath of unmineralized material in the plate (Figure 7).

The blue whale (72562) has the longest major plates on average (634.5 ± 27.8 mm), and they are a dark, blackish-blue color (Figure 2). Their minor plates are approximately three times smaller than the major plates, whereas the minor plates of the humpback whale (54806) measured around 10 times smaller than their major plates (Table 4). Blue whale major and minor plates had the largest plate spacing (12.9 ± 2.7 mm and 9.5 ± 1.6 mm, respectively) compared to the other species. Both measure four times larger than the major and minor spacing of the smallest plates, belonging to the minke whale (54808) (3.3 ± 0.4 mm and 2.0 ± 0.4 mm, respectively) (Figure 11, Table 4). Blue whale major plate fringe diameter is the largest of all the species (1.0 ± 0.2 mm), about twice that of humpback whales (0.5 ± 0.1 mm), which are the smallest. However, the blue whale's minor plate fringe diameter (0.4 ± 0.1 mm) is smaller than that of fin whale (54761), which is the biggest (0.6 ± 0.3 mm) (Figure 12, Table 4). Blue whale major plates varied the most in thickness between the labial and lingual sides; the labial side of the major plate measured over a mm thicker on average (4.9 ± 1.0 mm compared to 3.8 ± 0.8 mm) (Figure 13). Blue whale major plates were thinner than the gray whales, both labial and lingually (p = 3.91e−3) (Figure 13, Table 4, Supporting Information: Table 2). The largest rorquals, blue and fin whales, had similar fringe per cm densities for their minor plates (blue = 18.0 ± 1.6 cm, fin = 17.8 ± 3.5 cm) and were not found to be significantly different (Supporting Information: Table 2). While the minke and the humpback also have similar major plate fringe densities (22.6 ± 3.3 per cm and 16.5 ± 2.2 per cm, respectively; p = .16), the gray whale had far fewer fringes per cm (8.2 ± 1.5 cm) on their major plates compared to the other species (Table 4, Supporting Information: Table 2).

Fin whale baleen plates alternate bands of blue-gray and a creamy-yellow color (Figure 3). Unlike the other rorqual whales, the fin whales' major plates are similarly thick along the width of the plate, with the lingual and labial sides measuring the same thickness (3.6 ± 0.6 mm, 3.6 ± 0.8 mm) (Figure 13, Table 4). The fringe diameter of the fin whales' major (0.8 ± 0.2 mm) and minor plates (0.6 ± 0.3 mm) are similar to those of the gray whales, (major = 0.8 ± 0.1 mm, minor = 0.5 ± 0.1 mm) (Figure 12, Table 4).

Gray whale baleen is a light cream color. Gray whales have short major plates compared to the other samples in our data set (287.9 ± 55.8 mm) and were significantly different from all the other species, closest in size to those of the minke whale (196.9 ± 15.8 mm), despite their larger body size (Figure 4, Table 4). However, the major plates of the gray whales are the thickest of all the species, both from the lingual (4.7 ± 0.4 mm) and labial (5.3 ± 0.3 mm) sides. Gray whale plates display the largest difference in thickness between major and minor plates; the minor plates are 3.5 times thinner than the major plates (Figure 13, Table 4). Despite having the thickest major plates, gray whales have the fewest fringes per cm for both major (8.2 ± 1.5 mm) and minor plates (12.0 ± 2.0 mm) of all the five species (Table 4).

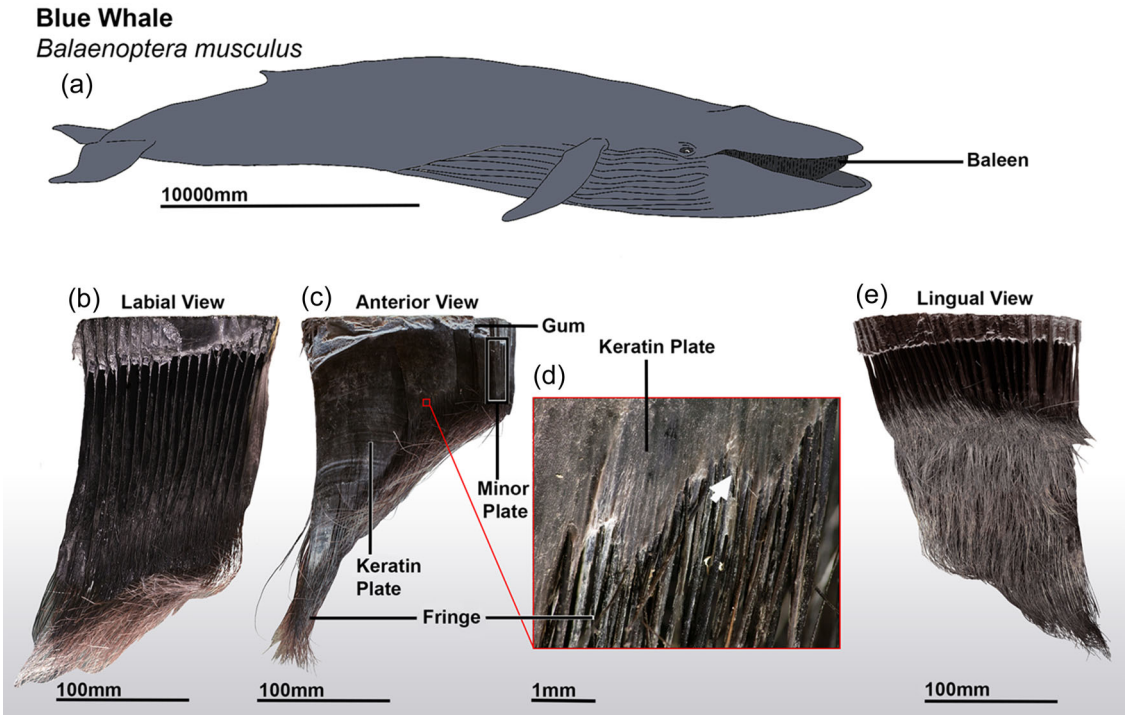

FIGURE 2 Gross morphology of blue whale (*Balaenoptera musculus*, C-517, juvenile) baleen. (a) Schematic of a blue whale showing the location of the baleen rack; (b, c, e) Labial, anterior, and lingual views showing the arrangement of baleen plates. Baleen is composed of larger major and minor plates that fray into a fringe. (d) Inset highlights the interface between the keratin plate and frayed fringes. Note the dark blue/black color.

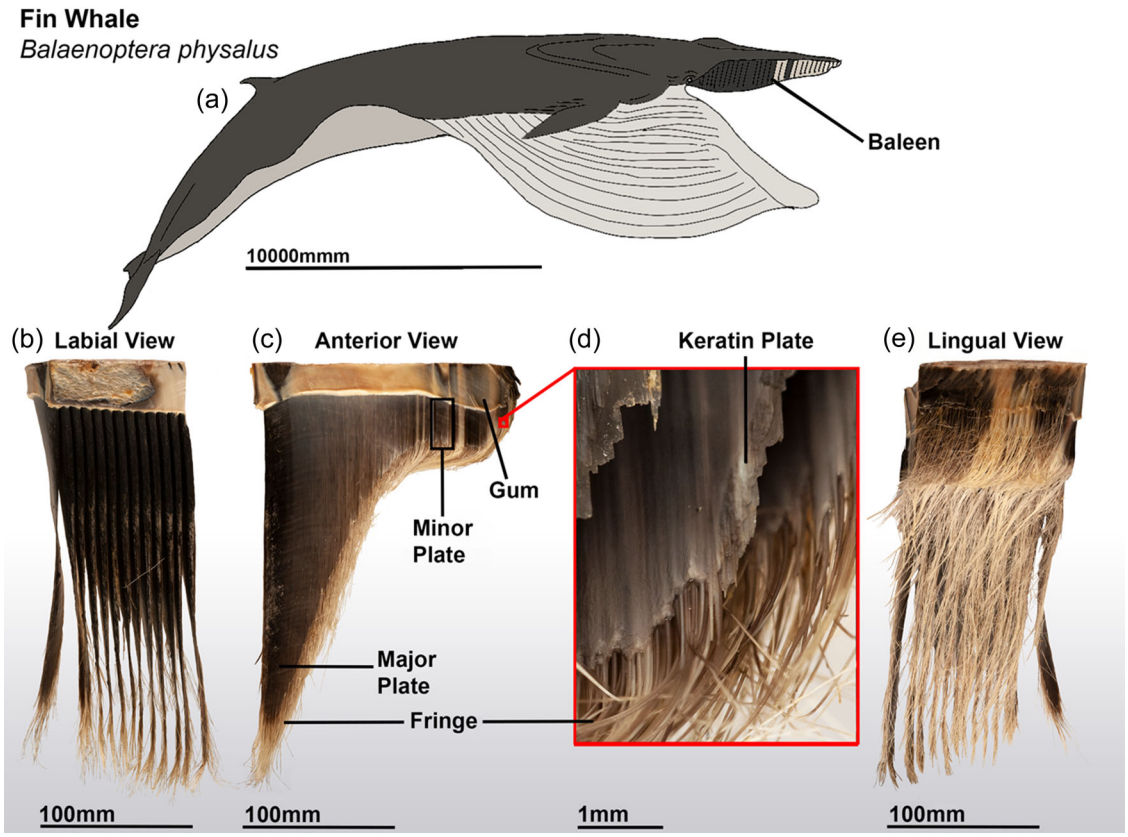

FIGURE 3 Gross morphology of fin whale (*Balaenoptera physalus*, C-669, juvenile) baleen. (a) Schematic of fin whale showing the location of the baleen rack; (b, c, e) Labial, anterior, and lingual views showing the arrangement of baleen plates. Baleen is composed of larger major and minor plates that fray into a fringe. (d) Inset highlights the interface between the keratin plate and frayed fringes. Note the alternating bands of blonde and black color.

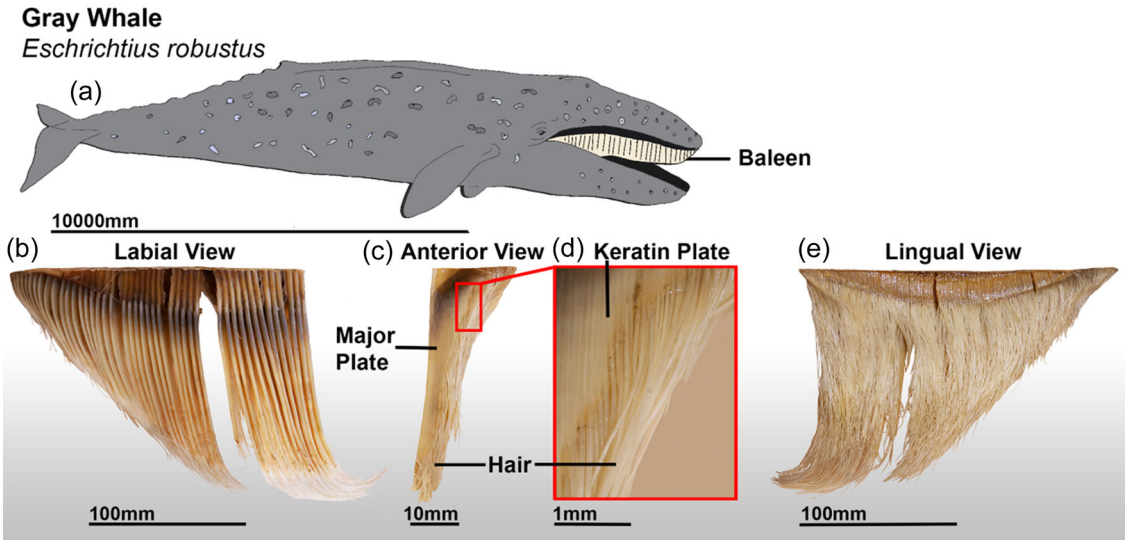

FIGURE 4 Gross morphology of gray whale (*Eschrichtius robustus*, R-2, unknown age) baleen. (a) Schematic of gray whale showing the location of the baleen rack; (b, c, e) Labial, anterior, and lingual views showing the arrangement of baleen plates. Baleen is composed of larger major and minor plates that fray into a fringe mat. (d) Inset highlights the interface between the keratin plate and frayed fringes.

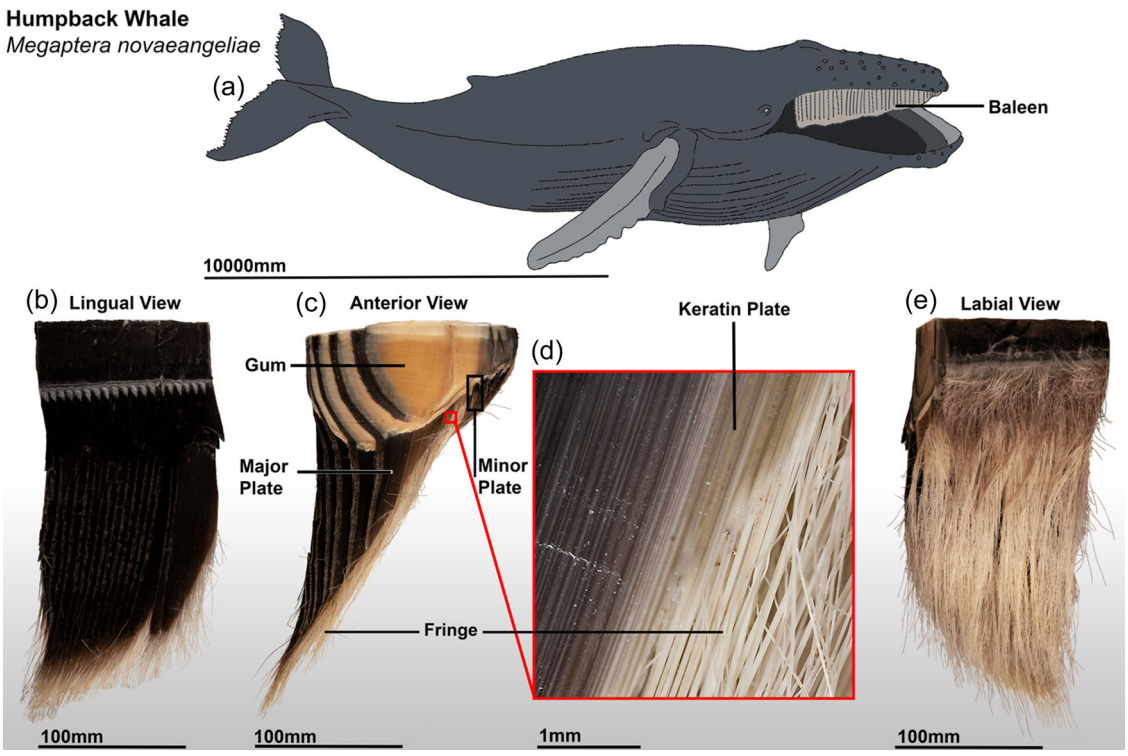

FIGURE 5 Gross morphology of humpback whale (*Megaptera novaeangliae*, C-634, juvenile) baleen. (a) Schematic of humpback whale showing the location of the baleen rack; (b, c, e) Labial, anterior, and lingual views showing the arrangement of baleen plates. (d) Inset highlights the interface between the keratin plate and frayed fringes.

Humpback whales have dark gray-brown baleen with cream-colored fringes (Figure 5). Humpback whales have the largest difference in spacing between their major and minor plates (8.4 ± 1.5 and 3.4 ± 0.3 mm, respectively), and the smallest major fringe diameter (0.5 ± 0.1 mm) (Figure 11, Table 4) of all the species. The major plates of the humpback are close in plate size (both length and width) to fin whales but significantly different in size to those of the gray and minke whales (Supporting Information: Table 2). They

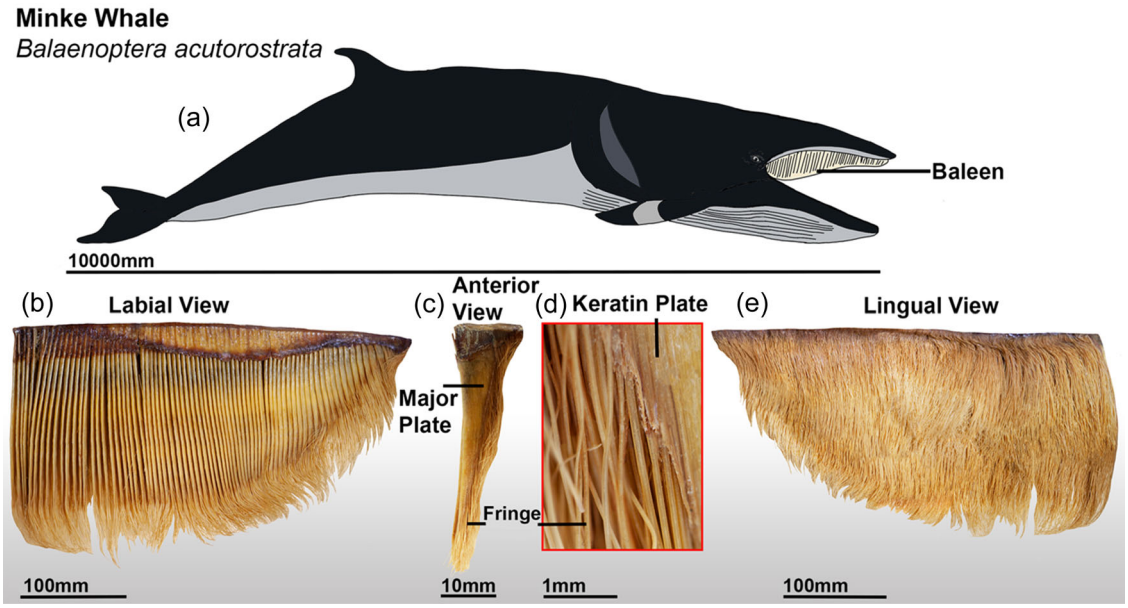

FIGURE 6 Gross morphology of minke whale (*Balaenoptera acutorostrata*, R-1, unknown age) baleen. (a) Schematic of a blue whale showing the location of the baleen rack; (b, c, e) Labial, anterior, and lingual views showing the arrangement of baleen plates. Baleen is composed of larger major and minor plates that fray into a fringe. (d) Inset highlights the interface between the keratin plate and frayed fringes.

FIGURE 7 Contrast-stained computed tomography scan of blue whale (*Balaenoptera musculus*, C-517, juvenile) baleen. (a) Minor plate stained with phosphotungstic acid, note the increased uptake of stain where the sheath breaks away from the fringe. (b) Transverse cut through the fringe of the minor plate above the break point showing diversity of fringe diameter. (c) Transverse cut through the keratin plate, showing fringes in the plate embedded in the matrix. The relationship between fringe and matrix density varies across species. Scale bar set to 10 mm.

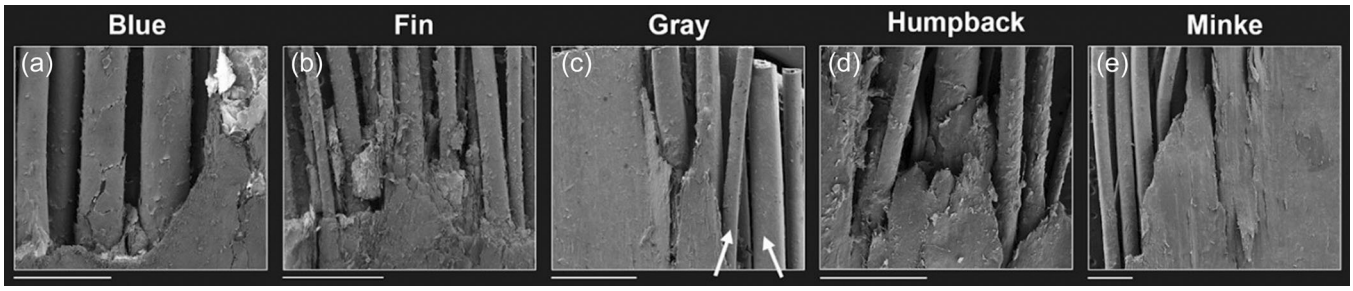

FIGURE 8 Scanning electron micrographs of baleen fringe (C-517, C-669, C-634, R-1, and R-2). (a–e) Show the interface where the plate breaks away from the fringes. Fringe diameters vary across species and major/minor plates (example shown in arrows). Scale bars set to 1 mm. (a, b, d) micrographs are from juvenile whales. (c, e) are from adult whales.

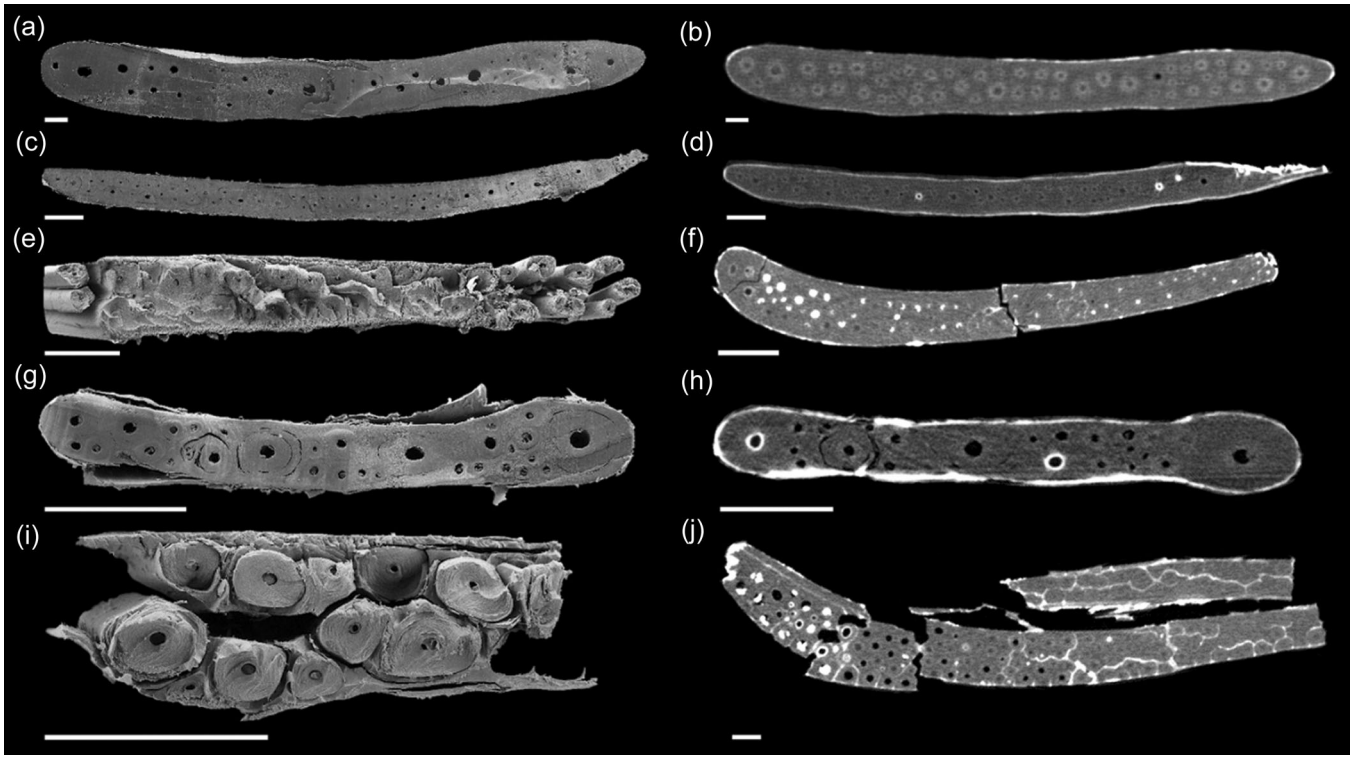

FIGURE 9 (a, b) are blue whale (*Balaenoptera musculus*, C-517), (c, d) are fin whale (*Balaenoptera physalus*, C-669), (e, f) are gray whale (*Esrichtius robustus*, R-2), (g, h) are humpback whale (*Megaptera novaeangliae*, C-634) and (i, j) are common minke whale (*Balaenoptera acutorostrata*, R-1). On the left, scanning electron micrographs (SEM) of the cross section of a keratin plate, and on the right, a computed tomography histology slice of the same piece of keratin plate shown. Fringes can be seen within the keratin plates in both types of images. The matrix breaking away from the fringes in concentric circles is seen within both images, but predominantly within the SEM images. All scale bars are 1 mm in length.

also have the greatest length difference between major and minor plates, minor plates are nearly 10 times smaller than major plates (Table 4). Humpback whales have the most fringes per cm in their minor plates across all species (28.3 ± 2.0 mm) (Table 4, Supporting Information: Table 2).

The common minke whale is the smallest rorqual in our data set and has cream colored baleen (Figure 6). Minke whale major plates are the shortest (196.9 ± 15.8 mm) and closest together of all the species (3.3 ± 0.4 mm), with their major plate spacing measuring more than four times smaller than that of the blue whale (Figure 11, Table 4). Minke whales have the thinnest major plates of the five species (lingual = 1.5 ± 0.2 mm, labial = 1.4 ± 0.3 mm), with a major plate fringe diameter of 0.7 ± 0.1 mm (Figures 12 and 13, Table 4). Minke whales also have the most fringes per cm in their major plates of all the whales (22.6 ± 3.3 mm) (Table 4).

Average fringe diameter varies across species and within a plate of a single individual—not all fringes inside a single plate are the same diameter or length. All species have larger major plate fringes than minor plate fringes, while the fringes of minor plates are more densely packed than those in the major plates (Table 4). The larger rorqual whales (blue, fin,

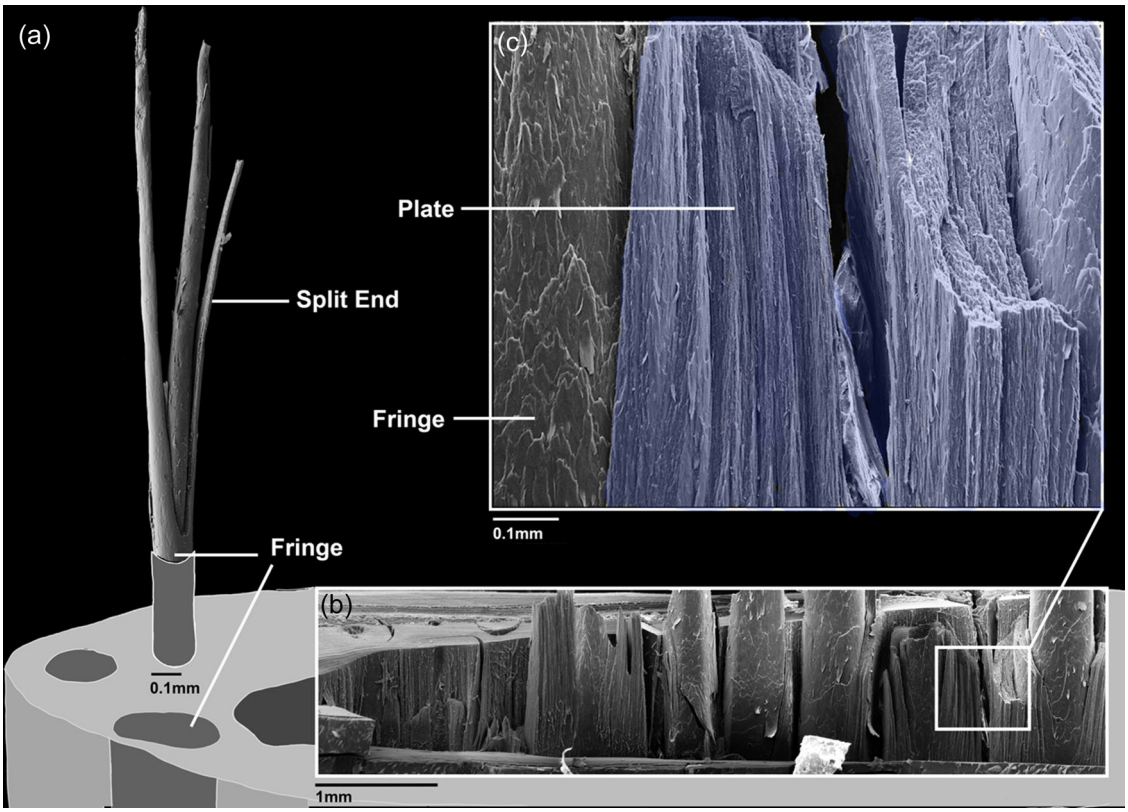

FIGURE 10 Scanning electron micrographs of sections of a blue whale (*Balaenoptera musculus*, juvenile, C-517) minor plate inserted into a recreation of plate anatomy. (a) Shows the split end of a fringe. (b, c) Shows a broken cross section of the minor plate, revealing the cylindrical fringes within the plate and the keratinized rings surrounding each fringe. (c) Highlights the structure of the plate.

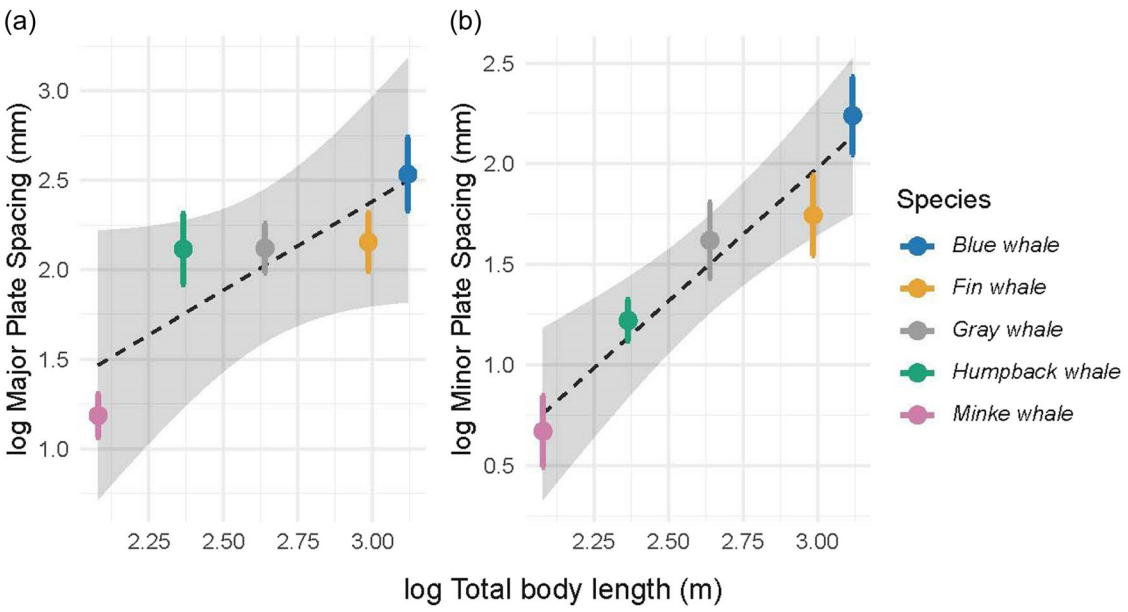

FIGURE 11 Major plate spacing (a) and minor plate spacing (b) versus total body length of each species of rorqual whale. Minor plate spacing exhibits hyperallometric scaling (slope = 1.327, 95% CI 1.129–1.525). Data is from Natural History Museum of Los Angeles County samples (Table 4).

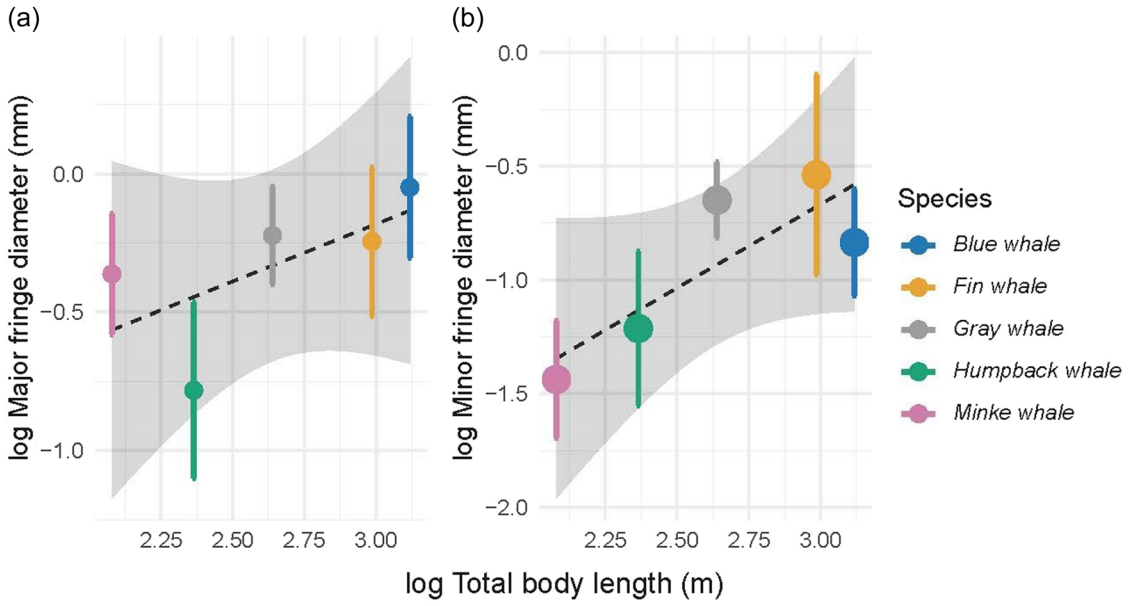

FIGURE 12 Plot showing the relationship between (a) major plate fringe diameter versus total body length of the rorqual for all five species and (b) minor plate fringe diameter versus total body length. Major and minor plate fringe diameter does not scale in proportion to body length, but instead exhibits hypoallometry (major = 0.415, 95% CI: 0.133–0.697; minor = 0.735, 95% CI: 0.450–1.020). Data is from Natural History Museum of Los Angeles County samples (Table 4).

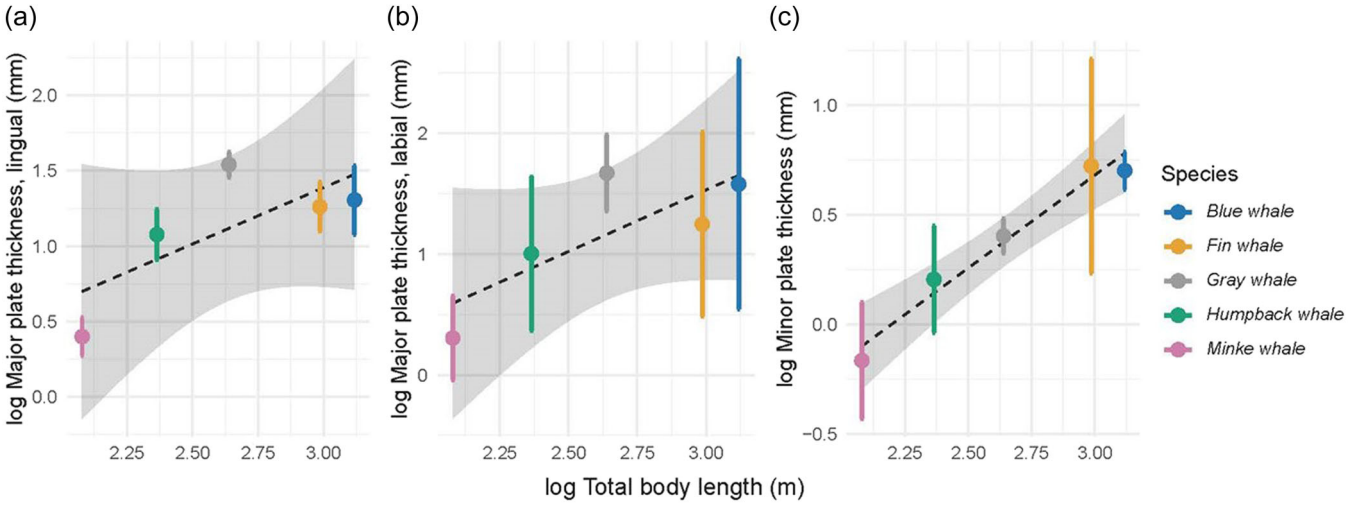

FIGURE 13 Major plate thickness ([a] lingual, [b] labial) and minor plate thickness (c) versus total body length of the rorqual for all five species. (a) Shows the thickness at the lingual side of the major plates and (b) shows the thickness at the labial side. The relationship between lingual major plate thickness and body length had a slope of 0.749 (95% CI: 0.358–1.139), while the relationship between labial major plate thickness and body length had a slope of 1.019 (95% CI: 0.577–1.461), and the relationship between minor plate thickness and body length had a slope of 0.848 (95% CI: 0.757–0.939). Data is from Natural History Museum of Los Angeles County samples (Table 4).

and gray whales) have fewer fringes per cm than the smaller rorquals (minke and humpback) in both the major and minor plates, with the gray whale having almost three times fewer fringes per cm than the minke whale (8.2 ± 1.5 and 22.6 ± 3.3 cm, respectively, $p = 5.62e^{-4}$) (Table 4, Supporting Information: Table 2) in the major plates. Both major and minor plates are degraded at the interface where fringes break free of the surrounding matrix. This degradation is particularly clear in contrast-stained CT, where PTA binds strongly to fringes at the point of emergence from the gum, and the matrix and fringes just below the emergence line (Figure 7, arrow). Emerging fringes are not the same height, and some appear snapped off while others are split (Figure 10).

In blue and humpback whales (C-517 and C-634) there were large vertical cracks through the outer sheath of the plates that extended to the gum line. These large cracks occur toward the lingual side of the major plates, separating the once large plate into smaller pieces—one the size of a minor plate and one an intermediate size between major and

TABLE 5 Prey preferences for all species, prey size estimates (mm), buccal volume (kg, s.d) (Kahane-Rapport et al., 2020), and buccal velocity (filtration time, kg, s.d) (Kahane-Rapport et al., 2020).

Species	Prey	Prey size estimate (mm)	Buccal volume (kg)	Buccal velocity (s)	Average species total body length (m)
Balaenoptera musculus	*Euphausia pacifica*	15.9–20.4 (Gómez-Gutiérrez et al., 2006); 14.4–23.6 (Du & Peterson, 2014)	88399.2 ± 43221.4	60.3 ± 20.4	22.4 ± 1.25
Balaenoptera physalus	*Euphausia pacifica*; *Engraulis mordax*	15.9–20.4 (Gómez-Gutiérrez et al., 2006); 14.4–23.6 (Du & Peterson, 2014); 120.0 (Cade et al., 2020)	57683.7 ± 22970.9	31.3 ± 11.6	18.9 ± 2.11
Eschrichtius robustus	Amphipods	15.0–20.0 (Oliver et al., 1983)	NA	NA	9.81–14.12 (Soledade Lemos et al., 2020)
Megaptera novaeangliae	*Euphausia pacifica*; *Engraulis mordax*	15.9–20.4 (Gómez-Gutiérrez et al., 2006); 14.4–23.6 (Du & Peterson, 2014); 120.0 (Cade et al., 2020)	25378.2 ± 11210.8	17.1 ± 6.0	11.5 ± 1.49
Balaenoptera acutorostrata	*Engraulis mordax*	120.0 (Cade et al., 2020)	2734.7 ± 1027.5[a]	8.9 ± 6.1[a]	

[a]Indicates buccal velocity and volumes for the Antarctic minke (Balaenoptera bonaerensis), not common minke whale. Data presently unavailable for gray whales.

TABLE 6 Hydraulic pore diameter for major and minor fringes from specimens C-517 (*B. musculus*), C-669 (*B. physalus*) and C-634 (*M. novaeangliae*).

Species	Fringe diameter (mm)	Epsilon (open fraction)	Volume of fringe (mm^3)	Surface area (mm^2)	Volume/SA d (s) (mm)	Sauter diameter S (v) (mm)	Hydraulic diameter d (h) (mm)	Average species total body length (m)
Balaenoptera musculus	0.98	0.58	0.75	3.08	0.25	24.49	0.222	22.4 ± 1.25
Balaenoptera physalus	0.81	0.41	0.52	2.54	0.20	29.62	0.093	18.9 ± 2.11
Megaptera novaeangliae	0.48	0.91	0.18	1.51	0.12	50	0.809	11.5 ± 1.49

Note: Average species total body length data from Kahane-Rapport et al. (2020).

minor plates. The smaller broken section of the major plate shifts laterally inside the gum, moving away from the position of its original major plate. This is seen in nine different major plates in the blue whale scan, and in five major plates in the humpback larger section scan. We did not see this in the minke and gray whales, though we note that we have not scanned large sections of baleen for those whales.

The hydraulic pore diameter for three species of rorqual ranged from 81 µm (humpback, C-634) to about 25 µm (blue whale, C-517). The blue whale (C-517), which had the largest diameter fringes, had a pore diameter almost three times smaller than humpback (C-634). Fin whale (C-669) hydraulic pore diameter was half as large as humpbacks' (Table 6).

TABLE 7 Slope, intercept, and confidence interval for relationships between log average morphological measurements and log average total length generated by linear models.

Model: log average morphological measurement ~ log average total length	Slope	Intercept	95% CI
Major fringe diameter	0.415	−1.426	0.133–0.697
Minor fringe diameter	0.735	−2.874	0.450–1.020
Major plate thickness, lingual	0.749	−0.858	0.358–1.139
Major plate thickness, labial	1.019	−1.526	0.577–1.461
Minor plate thickness	0.848	−1.864	0.757–0.939
Major plate spacing	0.994	−0.600	0.646–1.343
Minor plate spacing	1.327	−2.001	1.129–1.525
Major plate length	0.886	3.681	0.402–1.369
Minor plate length	1.485	0.057	0.891–2.078

Using linear models, we found that the relationship between major fringe diameter and body length across all species had a slope of 0.415 (95% CI 0.133–0.697) and the relationship between minor fringe diameter and body length across all species had a slope of 0.735 (95% CI 0.450–1.020) (Table 7); both major and minor fringe diameter are disproportionate to body length for all rorqual species. We found that the relationship between lingual major plate thickness and body length had a slope of 0.749 (95% CI 0.358–1.139), while the relationship between labial major plate thickness and body length had a slope of 1.019 (95% CI 0.577–1.461), and the relationship between minor plate thickness and body length had a slope of 0.848 (95% CI 0.757–0.939) (Table 7). The relationship between major plate spacing and body length had a slope of 0.994 (95% CI 0.646–1.343) and the relationship between minor plate spacing and body length had a slope of 1.327 (95% CI 1.129–1.525) (Table 7). Finally, we found that the relationship between major plate length and body length had a slope of 0.886 (95% CI 0.402–1.369) and the relationship between minor plate length and body length had a slope of 1.485 (95% CI 0.891–2.078) (Table 7). Overall, most measurements of baleen morphology exhibit hypoallometry (negative allometry) when compared to body size except for major plate thickness (labial), minor plate spacing, and minor plate length. (Figure 14).

4 | DISCUSSION

In all five rorqual species, the baleen rack is composed of keratin plates that fray into fringes which form a dense filtering mat. Some of these plates are larger and more labial than others, the major plates, while others are smaller and more lingual - the minor plates (Figures 2–6, inset B and E). All have an outer sheath composed of individual fringes

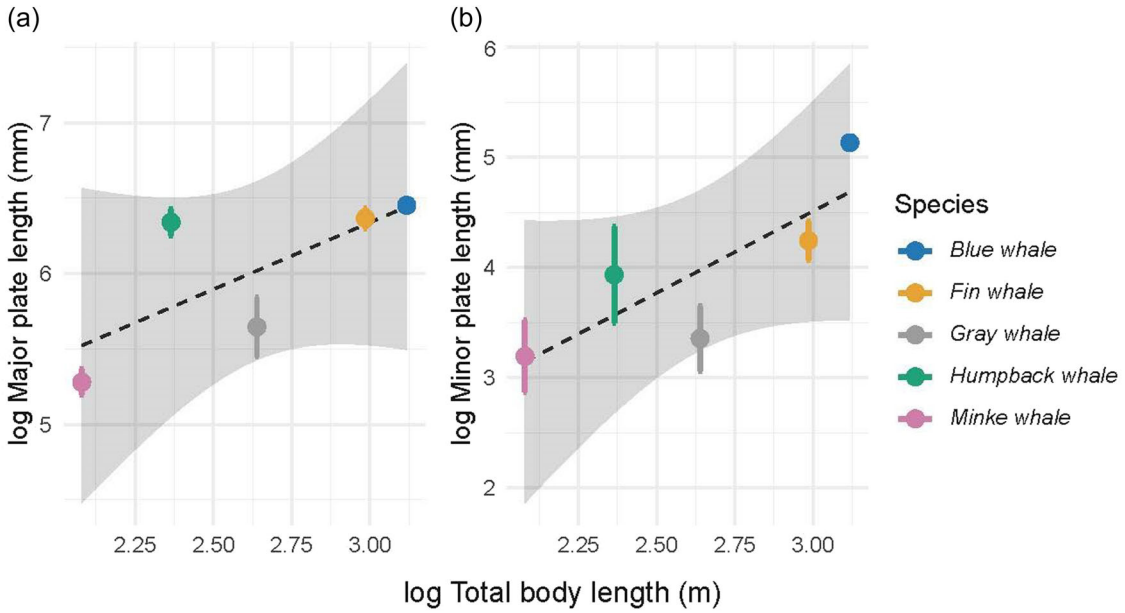

FIGURE 14 Plot showing the relationship between (a) major plate length and total body length of the rorqual for all five species and (b) the relationship between minor plate length and total body length. Major plate length does not scale in proportion to body length, but instead exhibits hypoallometry (slope = 0.886 95% CI: 0.402–1.369) while minor plate length does exhibits hyperallometry (slope = 1.485, 95% CI:0. 891–2.078). Data is from Natural History Museum of Los Angeles County samples (Table 4).

with some amount of matrix holding it all together. While the building blocks are similar, there are remarkable differences in baleen fringe diameter, fringe density, plate spacing, length, thickness, and color across the species. We expect differences in fringe diameter or density to convey something about filtration efficiency or prey choice, but it is less clear how color impacts the hydrodynamics of whale filtration. The relationship between material properties and the color of keratin has been most carefully explored in birds, where keratinous feathers with more melanin are harder and better at resisting damage (Barrowclough & Sibley, 1980; Bonser, 1995). Furthermore, hooves with increased levels of calcium were shown to be stronger (Fernando de Souza et al., 2019). Calcium levels are linked to the keratinization process, and this connection should prompt further work into the mineralization differences of different species baleen (Fernando de Souza et al., 2019). Blue whale baleen is almost black in color—a stark contrast to the light-colored fringes of humpback and minke baleen. It could be that the darker blue whale baleen—or any change in baleen color like the darker bands present in fin whale baleen—impacts this structure's ability to resist deformation during filtering or increases the toughness, making fracture more expensive.

Baleen is an unusual multifunctional structure—the broad flat plates channel and straighten flow, while the fringes filter and promote shear flow to clear the surface of accumulated prey (Werth & Potvin, 2016). The fringes of the filter are formed by the degradation of the plates (Werth et al., 2016). This single anatomical structure has two completely different roles, and the operative part of the filtering anatomy is generated by degradation of the flow shaping anatomy. The incoming water encounters baleen in the reverse of developmental order. The fringes emerge, perhaps through self-induced hydrodynamic flutter, from the thick plates, and the plates develop first in the gingiva of the jaws. The fringes are temporally older structures than the plates. The plate, with embedded fringes, is a solid structure, likely composed of alpha-keratin, and variably mineralized with crystalline hydroxyapatite (Pinto, 2011; Szewciw et al., 2010; Wang et al., 2019; Young et al., 2015).

Large cracks spanning the major plate from fringe to gum appear in the blue and humpback whales, which could be due to several different possibilities. First, these might be a postmortem artifact of the baleen removal process. As the baleen is flexed and twisted to dissect it from the gum tissue, cracks may be introduced. A second possibility is that when major plates reach a certain size, they can no longer resist the forces that shear and bend the plates during filtration, and these large cracks are a result of naturally occurring stresses. Smaller plates do not crack because the hydrodynamic forces are lower. Another possibility, related to the second one, is that hydrodynamic flutter occurs in large plates and the cracks are a response to this dynamic loading.

Fringes are the site of mineralization in the plate, appearing early and clearly in CT scans. They form a stiff core of the plate which, depending on the species, can be tightly packed with fringes or more sparsely arranged with swaths of presumably softer keratinous matrix between them (Pinto, 2011; Szewciw et al., 2010; Young et al., 2015). Our contrast CT data suggests something happens at the interface where fringes emerge from the solid plate that allows phosphotungstic acid to bind more strongly in this region. It could be that there is a biochemical signal, perhaps carried up the hollow shafts of the fringes, that triggers the emergence, or the already emerged fringes might vibrate in the flow generated by filtration. This vibration would stress the base of the fringes and could cause the material around the base to fracture and fall away. Thus, the flow itself would free the fringes that will act as filters from the surrounding matrix.

Once the fringes break free of the surrounding matrix, their functional imperatives swap from stiffening a larger structure to forming a network of fibers that together act to retain prey and direct surface flow (Werth et al., 2016). It is an unusual biological structure with two completely different loading regimes that act at the same time; fringes are both part of the larger structure shaping flow and when emerged, filtering prey items. Early in development, a mineralized, hollow fringe stiffens the baleen plate, and resists crack propagation (Vogel, 1988). At the same time, an older part of the same fringe has broken out of the plate and is loaded transversely as it acts in a mesh filter (Fudge et al., 2009; Thewissen et al., 2017). An analogous functional swap is seen in the teeth of bamboo sharks. When erect, the teeth are used for cutting fleshy prey, but lay flat when processing hard prey and take a compressive load at right angles to the load during cutting (Dean et al., 2008). We suggest that further investigation of baleen should seek to carefully describe the implications of fringe morphology on filter pore size and efficiency, and separately, the function of fringes in promoting the coordinated emergence of the filter from the flow-directing solid plates.

Filtration time increases with larger rorqual body size, a hypoallometric (negative allometry) relationship (Kahane-Rapport et al., 2020); larger whales engulf more water and filter water more slowly than smaller whales (Table 5). We found that there was a hypoallometric relationship between plate thickness and body length for all species, but a hyperallometric (positive allometry) relationship for plate spacing. The hyperallometry of plate spacing may offer some mechanical benefits that increase the speed of water processing (Table 5). We expected that fringe diameter would exhibit hyperallometry, with larger whales having fringes of greater diameter. However, fringe diameter, on both the major and minor plates, exhibits hypoallometry across the species (major fringe diameter $\propto$ length$^{0.45}$), meaning that larger whales have smaller than expected fringe diameter for their body length. The diameter and density of the fringe determines the hydraulic pore size of the filter mesh. There is a general trend that hydraulic pore diameter decreases with increasing body size; blue and fin whales have smaller pores than humpbacks (Table 6). While our sample size is too small to perform a linear model, we would expect a relationship of hypoallometry between hydraulic pore diameter and body length.

Although there is no obvious pore in a baleen mat, we can determine effective pore size using parameters measured from museum specimens and frozen baleen specimens, and experimentally conferred through modeling. In manufactured and biological filters, pore size is found by calculating some distance between filter elements, while an effective pore size is determined by both

anatomical and hydrodynamic variables (Riisgård & Larsen, 2001). Historically, there was an expectation that baleen pore size would be related to prey size (Nemoto, 1957, 1970; Tamura & Fujise, 2002). However, our findings do not show that hydraulic pore size correlates with prey size. Blue whales often forage on krill that have an average body length of 15.9–20.4 mm (Gómez-Gutiérrez et al., 2006), while their hydraulic pore size is 0.22 mm. This raises the possibility that differences in filter depth, fringe diameter, and fringe density may not be a proxy for prey size but instead, reflect changes in resistance through the filter that affect fluid flow. For example, a mesh of thick, uniform fringes should let prey escape and have minimal back-pressure; in contrast, a mat of fringe with highly variable diameter should have a smaller effective pore size, catch smaller prey, and have a higher back pressure. Greater back pressure can be useful for filtration because it drives shear flow that serves as a self-cleaning mechanism along the surface of the filter. Additionally, flow speed may also affect prey size retained. Paig-Tran et al. (2011) found that an animal's swimming speed will change to optimally target different size prey. The contraction of the expanded ventral groove blubber may be under muscular control by a foraging rorqual whale, allowing for different speeds of contraction and therefore increased control of the flow speed through the filter (Table 5).

While recent experimental and computational models have shown that cross-flow filtration is the most likely mechanism of balaenid filtration, the water flow patterns and filtration mechanism in rorqual whales remains poorly understood. It is important to note that the baleen fringes are not rigid, and constantly ebb and flow with the pressures of water. However, the fringes are also not endlessly flexible and therefore, void volume has bounds rooted in the anatomy of the fringe diameter and plate thickness. Our calculations of void fraction thus represent how this system should experience changes in overall pore in a dynamic system. We have presented here the first step for understanding the mechanism of filtration in rorqual whales by visualizing and quantifying the hierarchical anatomy of the baleen. Using our improved understanding of the interaction between the baleen filter elements, the major and minor plates, and the fringes, we suggest the next step is to experimentally model the filter mechanics by testing performance using different water flows and prey types.

ACKNOWLEDGMENTS

We would like to thank The Marine Mammal Center for providing the fresh baleen samples and the Natural History Museum of Los Angeles for providing the dry baleen samples. We thank Dr. Alexander Werth for his expertise and guidance. Funding for this work was provided by the National Science Foundation Division of Integrative Organismal Systems grant #1932757 and the National Science Foundation Postdoctoral Research Fellowship in Biology grant #2209494. Funding for this work was also provided by the American Cetacean Society Los Angeles and Monterey Bay chapters and the Stephen and Ruth Wainwright Endowment Fellowship.

CONFLICT OF INTEREST STATEMENT

The authors declare no conflict of interest.

DATA AVAILABILITY STATEMENT

The data that support the findings of this study are openly available in GitHub at https://github.com/shirelkr/baleen_morphology. All CT scans are available on MorphoSource at https://www.morphosource.org/projects/000458964?locale=en

PEER REVIEW

The peer review history for this article is available at https://www.webofscience.com/api/gateway/wos/peer-review/10.1002/jmor.21574.

ORCID

Karly E. Cohen https://orcid.org/0000-0001-6556-5414
Jeremy A. Goldbogen https://orcid.org/0000-0002-4170-7294
Adam P. Summers https://orcid.org/0000-0003-1930-9748
E. W. Misty Paig-Tran https://orcid.org/0000-0001-9317-4621
Shirel R. Kahane-Rapport https://orcid.org/0000-0002-5208-1100

REFERENCES

Árnason, Ú., Lammers, F., Kumar, V., Nilsson, M. A., & Janke, A. (2018). Whole-genome sequencing of the blue whale and other rorquals finds signatures for introgressive gene flow. *Science Advances*, *4*, eaap9873.

Barrowclough, G. F., & Sibley, F. C. (1980). Feather pigmentation and abrasion: Test of a hypothesis. *The Auk*, *97*(4), 881–883. https://doi.org/10.1093/auk/97.4.881

Bhave, R. R. (1997). Cross flow filtration. In H. C. Vogel, & C. L. Todaro (Eds.), *Fermentation biochemical engineering handbook* (pp. 271–322). Noyes Publications.

Bonser, R. H. C. (1995). Melanin and the abrasion resistance of feathers. *Condor*, *97*(2), 590–591. https://doi.org/10.2307/1369048

Brower, A. A., Ferguson, M. C., Schonberg, S. V., Jewett, S. C., & Clarke, J. T. (2017). Gray whale distribution relative to benthic invertebrate biomass and abundance: Northeastern Chukchi Sea 2009–2012. *Deep Sea Research Part II: Topical Studies in Oceanography*, *144*, 156–174.

Cade, D. E., Carey, N., Domenici, P., Potvin, J., & Goldbogen, J. A. (2020). Predator-informed looming stimulus experiments reveal how large filter feeding whales capture highly maneuverable forage fish. *Proceedings of the National Academy of Sciences*, *117*(1), 472–78. https://doi.org/10.1073/pnas.1911099116

Cade, D. E., Friedlaender, A. S., Calambokidis, J., & Goldbogen, J. A. (2016). Kinematic diversity in Rorqual whale feeding mechanisms. *Current Biology*, *26*, 2617–2624.

Cohen, K. E., Hernandez, L. P., Crawford, C. H., & Flammang, B. E. (2018). Channeling vorticity: Modeling the filter-feeding mechanism in silver carp using μcT and 3D PIV. *Journal of Experimental Biology*, *221*, jeb183350.

Dean, M. N., Ramsay, J. B., & Schaefer, J. T. (2008). Tooth reorientation affects tooth function during prey processing and tooth ontogeny in the lesser electric ray, *Narcine brasiliensis*. *Zoology*, *111*, 123–134.

Du, X., & Peterson, W. (2014). Feeding rates and selectivity of adult euphausia pacifica on natural particle assemblages in the coastal upwelling zone off oregon, USA, 2010. *Journal of Plankton Research*, *36*(4), 1031–1046. https://doi.org/10.1093/plankt/fbu027

Ekdale, E. G., & Deméré, T. A. (2022). Neurovascular evidence for a co-occurrence of teeth and baleen in an Oligocene mysticete and the transition to filter-feeding in baleen whales. *Zoological Journal of the Linnean Society*, *194*, 395–415.

Fernando de Souza, A., Schade, J., Laus, R., Alves Moreira, M., Müller, T. R., & Fonteque J. H. (2019). Differences in mineral concentrations on hooves of horses, mules and donkeys. *Brazilian Journal of Veterinary Science*, *26*, 93–97. https://doi.org/10.4322/rbcv.2019.017

Fudge, D. S., Szewciw, L. J., & Schwalb, A. N. (2009). Morphology and development of Blue Whale Baleen: An annotated translation of Tycho Tullberg's Classic 1883 paper. *Aquatic Mammals*, *35*, 226–252.

Gatesy, J., Ekdale, E. G., Deméré, T. A., Lanzetti, A., Randall, J., Berta, A., El Adli, J. J., Springer, M. S., & McGowen, M. R. (2022). Anatomical, ontogenetic, and genomic homologies guide reconstructions of the teeth-to-Baleen transition in mysticete whales. *Journal of Mammalian Evolution*, *29*, 891–930.

Gatesy, J., Geisler, J. H., Chang, J., Buell, C., Berta, A., Meredith, R. W., Springer, M. S., & McGowen, M. R. (2013). A phylogenetic blueprint for a modern whale. *Molecular Phylogenetics and Evolution*, *66*, 479–506.

Geisler, J. H., Boessenecker, R. W., Brown, M., & Beatty, B. L. (2017). The origin of filter feeding in whales. *Current Biology*, *27*, 2036–2042.e2.

Goldbogen, J., Pyenson, N., & Shadwick, R. (2007). Big gulps require high drag for fin whale lunge feeding. *Marine Ecology Progress Series*, *349*, 289–301.

Goldbogen, J. A., Cade, D. E., Calambokidis, J., Friedlaender, A. S., Potvin, J., Segre, P. S., & Werth, A. J. (2017). How Baleen whales feed: The biomechanics of engulfment and filtration. In*Annual review of marine science* (Vol. 9, pp. 367–386). Annual Reviews.

Goldbogen, J. A., Hazen, E. L., Friedlaender, A. S., Calambokidis, J., DeRuiter, S. L., Stimpert, A. K., & Southall, B. L. (2015). Prey density and distribution drive the three-dimensional foraging strategies of the largest filter feeder. *Functional Ecology*, *29*, 951–961.

Gómez-Gutiérrez, J., Feinberg, L., Shaw, T., & Peterson, W. (2006). Variability in brood size and female length of *Euphausia pacifica* among three populations in the North Pacific. *Marine Ecology Progress Series*, *323*, 185–194.

Jensen, M. M., Saladrigas, A. H., & Goldbogen, J. A. (2017). Comparative three-dimensional morphology of Baleen: Cross-sectional profiles and volume measurements using CT images. *The Anatomical Record*, *300*, 1942–1952.

Kahane-Rapport, S. R., Savoca, M. S., Cade, D. E., Segre, P. S., Bierlich, K. C., Calambokidis, J., & Goldbogen, J. A. (2020). Lunge filter feeding biomechanics constrain rorqual foraging ecology across scale. *Journal of Experimental Biology*, *223*, jeb224196. https://doi.org/10.1242/jeb.224196

Kahane-Rapport, S. R., & Goldbogen, J. A. (2018). Allometric scaling of morphology and engulfment capacity in rorqual whales. *Journal of Morphology*, *279*, 1256–1268.

Kassambara, A. (2021). *rstatix: Pipe-friendly framework for basic statistical tests*. https://cran.r-project.org/web/packages/rstatix/index.html

Kerkhoff, A. J., & Enquist, B. J. (2009). Multiplicative by nature: Why logarithmic transformation is necessary in allometry. *Journal of Theoretical Biology*, *257*, 519–521.

Lambertsen, R. H. (1983). Internal mechanism of rorqual feeding. *Journal of Mammalogy*, *64*, 76–88.

Lammers, F., Blumer, M., Rücklé, C., & Nilsson, M. A. (2019). Retro-phylogenomics in rorquals indicate large ancestral population sizes and a rapid radiation. *Mobile DNA*, *10*, 5.

Matthews, L. H., & Parker, H. W. (1950). Notes on the anatomy and biology of the Basking shark (*Cetorhinus maximus* (Gunner). *Proceedings of the Zoological Society of London*, *120*, 535–576.

McGowen, M. R., Tsagkogeorga, G., Álvarez-Carretero, S., dos Reis, M., Struebig, M., Deaville, R., Jepson, P. D., Jarman, S., Polanowski, A., Morin, P. A., & Rossiter, S. J. (2020). Phylogenomic resolution of the Cetacean tree of life using target sequence capture. *Systematic Biology*, *69*, 479–501.

Misty paig-Tran, E. W., & Summers, A. P. (2014). Comparison of the structure and composition of the branchial filters in suspension feeding elasmobranchs. *The Anatomical Record*, *297*, 701–715.

Nemoto, T. (1957). Foods of baleen whales in the northern Pacific. *The Scientific Reports of the Whales Reseach Institute*, *12*, 33–89.

Nemoto, T. (1970). Feeding pattern of baleen whales in the ocean. In J. H. Steele (Ed.), *Marine food chains* (pp. 241–252). University of California Press.

Oliver, J. S., Slaitery, P. N., Silberstein, M. A., & O'connor, E. F. (1983). A comparison of gray whales, eschrichtius robustus, feeding in the Bering Sea and Baja California. *Fishery Bulletin*, *81*(3), 513–522.

Paig-Tran, E. W. M., Bizzarro, J. J., Strother, J. A., & Summers, A. P. (2011). Bottles as models: Predicting the effects of varying swimming speed and morphology on size selectivity and filtering efficiency in fishes. *Journal of Experimental Biology*, *214*, 1643–1654.

Paig-Tran, E. W. M., Kleinteich, T., & Summers, A. P. (2013). The filter pads and filtration mechanisms of the devil rays: Variation at macro and microscopic scales: Filter pads and filtration mechanisms of devil rays. *Journal of Morphology*, *274*, 1026–1043.

Pinto, S. J. D. (2011). *On the filtration mechanisms and oral anatomy of lunge-feeding baleen whales* [Master of Science, The University of British Columbia]. Vancouver.

Pivorunas, A. (1977). The fibrocartilage skeleton and related structures of the ventral pouch of Balaenopterid whales. *Journal of Morphology*, *151*, 299–313.

Potvin, J., & Werth, A. J. (2017). Oral cavity hydrodynamics and drag production in Balaenid whale suspension feeding. *PLoS One*, *12*, e0175220.

Riisgård, H. U., & Larsen, P. S. (2001). Minireview: Ciliary filter feeding and bio-fluid mechanics—present understanding and unsolved problems. *Limnology and Oceanography*, *46*, 882–891.

Ripperger, S., Gösele, W., Alt, C., & Loewe, T. (2013). Filtration, 1. Fundamentals. In C. Ley, (Ed.), *Ullmann's Encyclopedia of industrial chemistry* (pp. 1–38). John Wiley & Sons, Ltd.

Roberts, T. R. (2012). *Systematics, biology, and distribution of the species of the oceanic oarfish genus Regalecus (Teleostei, Lampridiformes, Regalecidae)*. French National Museum of Natural History.

Rolfe, S., Pieper, S., Porto, A., Diamond, K., Winchester, J., Shan, S., Kirveslahti, H., Boyer, D., Summers, A., & Maga, A. M. (2021). SlicerMorph: An open and extensible platform to retrieve, visualize and analyse 3D morphology. *Methods in Ecology and Evolution*, *12*(10), 1816–1825. https://doi.org/10.1111/2041-210X.13669

Rubenstein, D. I., & Koehl, M. A. R. (1977). The mechanisms of filter feeding: Some theoretical considerations. *The American Naturalist*, *111*, 981–994.

Sanderson, S. L., Cheer, A. Y., Goodrich, J. S., Graziano, J. D., & Callan, W. T. (2001). Crossflow filtration in suspension-feeding fishes. *Nature*, *412*, 439–441.

Sanderson, S. L., Roberts, E., Lineburg, J., & Brooks, H. (2016). Fish mouths as engineering structures for vortical cross-step filtration. *Nature Communications*, *7*, 11092.

Sasaki, T., Nikaido, M., Hamilton, H., Goto, M., Kato, H., Kanda, N., Pastene, L. A., Cao, Y., Fordyce, R. E., Hasegawa, M., & Okada, N. (2005). Mitochondrial phylogenetics and evolution of mysticete whales. *Systematic Biology*, *54*, 77–90.

Schneider, C. A., Rasband, W. S., & Eliceiri, K. W. (2012). NIH image to ImageJ: 25 years of image analysis. *Nature Methods*, *9*, 671–675.

Shadwick, R. E., Potvin, J., & Goldbogen, J. A. (2019). Lunge feeding in rorqual whales. *Physiology*, *34*, 409–418.

Soledade Lemos, L., Burnett, J. D., Chandler, T. E., Sumich, J. L., & Torres L. G. (2020). Intra- and inter-annual variation in gray whale body condition on a foraging ground. *Ecosphere*, *11*(4), e03094. https://doi.org/10.1002/ecs2.3094

Stiefel, K. M. (2021). Evolutionary trends in large pelagic filter-feeders. *Historical Biology*, *33*, 1477–1488.

Storm, T. J., Nolan, K. E., Roberts, E. M., & Sanderson, S. L. (2020). Oropharyngeal morphology related to filtration mechanisms in suspension-feeding American shad (Clupeidae). *Journal of Experimental Zoology Part A: Ecological and Integrative Physiology*, *333*, 493–510.

Szewciw, L. J., de Kerckhove, D. G., Grime, G. W., & Fudge, D. S. (2010). Calcification provides mechanical reinforcement to whale baleen α-keratin. *Proceedings of the Royal Society B: Biological Sciences*, *277*, 2597–2605.

Tamura, T. (2002). Geographical and seasonal changes of the prey species of minke whale in the Northwestern Pacific. *ICES Journal of Marine Science*, *59*, 516–528.

Thewissen, J. G. M., Hieronymus, T. L., George, J. C., Suydam, R., Stimmelmayr, R., & McBurney, D. (2017). Evolutionary aspects of the development of teeth and baleen in the bowhead whale. *Journal of Anatomy*, *230*, 549–566.

Vogel, S. (1988). *Life's devices: The physical world of animals and plants*. Princeton University Press.

Wang, B., Sullivan, T. N., Pissarenko, A., Zaheri, A., Espinosa, H. D., & Meyers, M. A. (2019). Lessons from the ocean: Whale Baleen fracture resistance. *Advanced Materials*, *31*, 1804574.

Werth, A. J. (2000). Feeding in marine mammals. In K. Schwenk (Ed.), *Feeding: Form, function, and evolution in tetrapod vertebrates* (pp. 487–526). Academic Press.

Werth, A. J. (2001). How do mysticetes remove prey trapped in baleen. *Bulletin of the Museum of Comparative Zoology*, *156*, 189–203.

Werth, A. J., Harriss, R. W., Rosario, M. V., George, J. C., & Sformo, T. L. (2016). Hydration affects the physical and mechanical properties of baleen tissue. *Royal Society Open Science*, *3*, 160591.

Werth, A. J., & Ito, H. (2017). Sling, scoop, and squirter: Anatomical features facilitating prey transport, processing, and swallowing in Rorqual whales (Mammalia: Balaenopteridae): Rorqual oral transporT. *The Anatomical Record*, *300*, 2070–2086.

Werth, A. J., & Potvin, J. (2016). Baleen hydrodynamics and morphology of cross-flow filtration in Balaenid whale suspension feeding. *PLoS One*, *11*, e0150106.

Werth, A. J., Potvin, J., Shadwick, R. E., Jensen, M. M., Cade, D. E., & Goldbogen, J. A. (2018). Filtration area scaling and evolution in mysticetes: Trophic niche partitioning and the curious cases of sei and pygmy right whales. *Biological Journal of the Linnean Society*, *125*, 264–279.

Werth, A. J., Rita, D., Rosario, M. V., Moore, M. J., & Sformo, T. L. (2018). How do baleen whales stow their filter? A comparative biomechanical analysis of baleen bending. *Journal of Experimental Biology*, *221*, jeb189233.

Werth, A. J., Straley, J. M., & Shadwick, R. E. (2016). Baleen wear reveals intraoral water flow patterns of mysticete filter feeding. *Journal of Morphology*, *277*, 453–471.

Wickham, H., Averick, M., Bryan, J., Chang, W., McGowan, L., François, R., Grolemund, G., Hayes, A., Henry, L., Hester, J., Kuhn, M., Pedersen, T., Miller, E., Bache, S., Müller, K., Ooms, J., Robinson, D., Seidel, D., Spinu, V., … Yutani, H. (2019). Welcome to the Tidyverse. *Journal of Open Source Software*, *4*, 1686.

Wickham, H., François, R., Henry, L., & Muller, K. (2022). *dplyr: A grammar of data manipulation*. https://dplyr.tidyverse.org

Williamson, G. (1973). Counting and measuring baleen and ventral grooves of whales. *Scientific Reports of the Whales Research institute*, *25*, 279–292.

Young, S., Deméré, T. A., Ekdale, E. G., Berta, A., & Zellmer, N. (2015). Morphometrics and structure of complete Baleen racks in gray whales (*Eschrichtius robustus*) from the eastern north Pacific Ocean: Morphometrics and structure of complete baleen racks. *The Anatomical Record*, *298*, 703–719.

SUPPORTING INFORMATION

Additional supporting information can be found online in the Supporting Information section at the end of this article.

How to cite this article: Vandenberg, M. L., Cohen, K. E., Rubin, R. D., Goldbogen, J. A., Summers, A. P., Paig-Tran, E. W. M., & Kahane-Rapport, S. R. (2023). Formation of a fringe: A look inside baleen morphology using a multimodal visual approach. *Journal of Morphology*, *284*, e21574. https://doi.org/10.1002/jmor.21574